Journal of ELECTRONIC MATERIALS, Vol. 50, No. 3, 2021
https://doi.org/10.1007/s11664-020-08616-7

ORIGINAL RESEARCH ARTICLE

Electrochemical Analysis of Indigo Carmine in Food and Water Samples Using a Poly(Glutamic Acid) Layered Multi-walled Carbon Nanotube Paste Electrode

N. HAREESHA,[1] J.G. MANJUNATHA ,[1,3] B.M. AMRUTHA,[1,2] P.A. PUSHPANJALI,[1] M.M. CHARITHRA,[1] and N. PRINITH SUBBAIAH[1]

1.—Department of Chemistry, FMKMC College, Mangalore University Constituent College, Madikeri, Karnataka, India. 2.—Department of Chemistry, N.M.A.M. Institute of Technology, Visvesvaraya Technological University, Nitte, Udupi District, Belgavi, Karnataka 574110, India. 3.—e-mail: manju1853@gmail.com

Some colourants are hazardous to living organisms. Hence, a powerful and fast methodology is required for the analysis of those colourants in food and water samples. A modest electrochemically polymerised glutamic acid layered multi-walled carbon nanotube paste electrode [P(GA)LMWCNTPE] was functionalised for the sensing of indigo carmine (IC) by the differential pulse voltammetry (DPV) and cyclic voltammetry (CV) approaches. Within the optimised experimental conditions, the P(GA)LMWCNTPE holds an acceptable and high rate of electro-catalytic activity towards the redox behaviour of IC. The projected P(GA)LMWCNTPE shows a decent selectivity for IC in the presence of methyl orange. The modified sensor shows an acceptable linear growth between oxidative peak current and concentration in both CV and DPV methods with fine limit of detection values of 4.2 μM and 0.36 μM, respectively. Additionally, the developed sensor was effectively applied to detect IC in food and water samples. The morphological and surface activities of the modified and unmodified electrodes were determined through field emission scanning electron microscopy, electrochemical impedance spectroscopy, and CV techniques. The P(GA)LMWCNTPE requires a simple preparation procedure and is low-cost, with acceptable storage stability, sensitivity, and reproducibility.

(Received September 2, 2020; accepted November 6, 2020; published online January 4, 2021)

Graphic Abstract

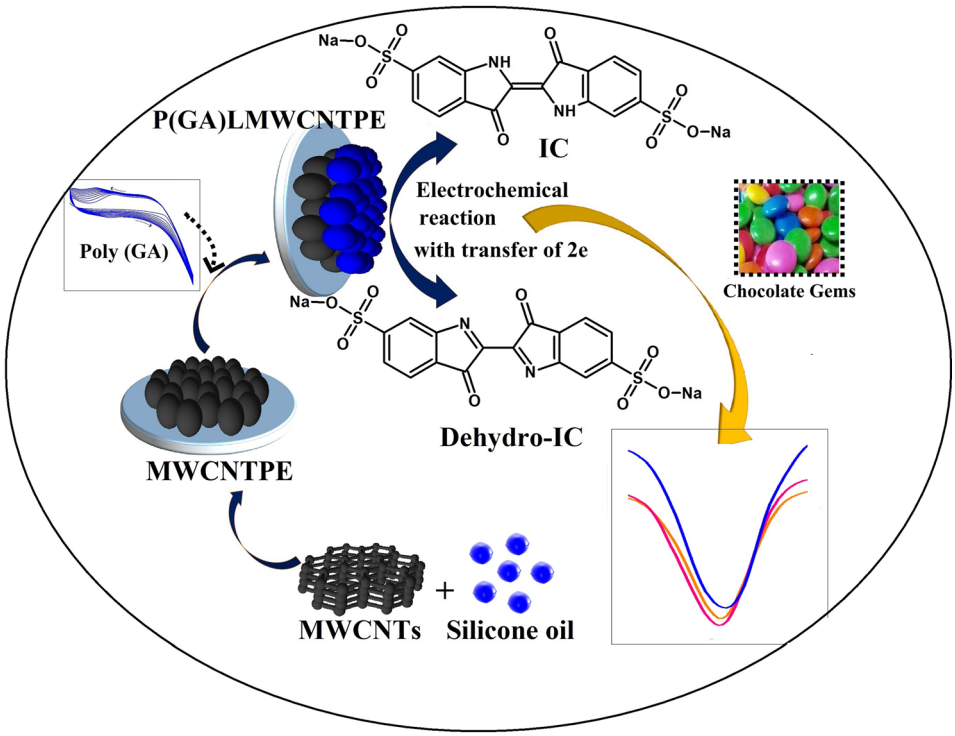

Key words: Electropolymerised glutamic acid, indigo carmine, electrochemical impedance spectroscopy, multi-walled carbon nanotubes, voltammetry

INTRODUCTION

Dyes are most imperative substances, utilized as synthetic colouring agents in food, beauty products, clothes, papers, medicines, furniture, photographs, paints, leather, electronic materials, and also in the staining of samples in forensic investigations.[1–4] Numerous estimations have reported that more than ten thousand various colouring dyes are utilised in various industries, and more than 70 micro-tons of artificial colourants are manufactured in the global market. Unfortunately, 10% to 50% of these dyes are wasted during the dyeing and finishing processes, and massive quantities of wasted dyes are directly released to the environment. Most of the released dyes are noxious and mutagenic, with numerous negative impacts on the environment including oxygen deficiency, impeded sunlight penetration (leads to lowering of photosynthetic activity), and variation in biological oxygen demand, pH, salinity of the soil, and chemical oxygen demand, and affecting fundamental uses such as irrigation and drinking water. These defects cause many deadly diseases among living organisms. Even less than 1.0 mg of dye in one litre of water hazardously affects the aquatic environment.[5]

Indigo carmine (IC) or 3,3′-dioxo-2,2′-bisindolyden-5,5′-disulfonic acid disodium salt is a water-soluble natural hydrophilic dye occurring through natural indigo sulfonation. IC is used in some very important applications, such as ozone and superoxide detection, pH indication in redox reactions, preparation of medicinal capsules, and colouring of food, beverage, and denim fabric products.[6] Also, IC is significantly used for a variety of treatments such as gastric cancer,[7] transurethral resection and vesicoureteral reflux by locating ureteral orifices (destroys muscle fibres, leading to upper tract urothelial carcinoma development),[8,9] obstetric surgery, and chemotherapy of hepatic tumours.[10] Some of the earlier reports revealed that the highest allowed range of IC in the normal living body is from 100 mg/kg to 300 mg/kg body weight.[11] Nevertheless, the anomaly of IC concentration in water and food samples stimulates some insensitive effects in

living species, such as hereditary problems, invariable blood pressure, hypertension, urticaria, eye problems, bronchospasm, and cancer-related tumour growth.[12–18] Hence, IC inspection and overprotection in water and food samples are most essential in an easy and faster way.

In previous studies, various analytical approaches have been reported for IC analysis, such as chemiluminescence,[19] thin-layer chromatography,[20] spectrophotometry,[21] high-performance liquid chromatography,[22] flow amperometry,[23] and tandem mass spectrometry.[24] These techniques are monotonous, high-priced, time-consuming, and require sample preparation with complicated instrumentation and handling. Consequently, these techniques are probably less appropriate for routine IC assessment. However, electrochemical methods are the most effective practical tools for the sensing of electrochemically active molecules because of their high sensitivity, selectivity, stability, quick and potent response, low cost, reduced time consumption, easy handling, and easy optimization procedures in the available laboratory circumstances.[25–29] These electrochemical methods need a working electrode to enhance the sensing activity with a high peak current.

Nowadays, multi-walled carbon nanotubes (MWCNTs) are the best sensing materials for the investigation of bioactive and electroactive molecules because they show some special features such as elevated mechanical potency, finer electrical conductivity, lofty dynamic surface area, high chemical steadiness, exceptional electronic behaviours, simple preparation, low cost, and execution of extremely accurate and steady voltammograms.[17,30] Hence, MWCNTs are functionalized as a significant sensing material for this work.

Polymer amino acid-based sensors have recently captured much attention for use in electrochemical investigations. In particular, polymerised glutamic acid [poly(GA)] shows higher biocompatibility, stability, reproducibility, sensitivity, a non-toxic nature, bio-medicinal activity, and strong adherence towards the surface of the sensor, and offers more surface sites with conducting bridges.[31] Therefore, in this work poly(GA) is used as a chemical modifier at the exterior of a multi-walled carbon nanotube paste electrode (MWCNTPE) to provide high conductivity and catalytic activity.

As from the brief literature study, there are no earlier reported works on the electrochemical sensing of IC in both commercial and real (food and water) samples on the conductive surface of P(GA)LMWCNTPE through the cyclic voltammetry (CV) and differential pulse voltammetry (DPV) methods. The simultaneous analysis of IC with methyl orange (MO) was examined using the DPV method. This data certifies the analytical applications and informational validations for the inspection of food and water quality.

EXPERIMENTAL

Chemicals and Reagents

IC (analyte) and GA were purchased from Molychem, India. $Na_2HPO_4.2H_2O$, $NaH_2PO_4.H_2O$, and $K_4[Fe(CN)_6]\cdot 3H_2O$ were procured from HiMedia, India. Silicone oil and KCl were bought from Nice Chemicals, India. MWCNTs (with external diameter and length of 30–50 nm and 10–30 μm, respectively) were purchased from Sisco Research Laboratories, India. MO was procured from British Drug Houses, England. The food sample (Gems chocolates) was purchased from a nearby general store. These chemicals were of analytical reagent quality and utilised with no additional refinement. All the chemical solutions of the appropriate concentration were prepared by dissolving a calculated quantity of compound in distilled water. The entire investigation was done at the laboratory temperature of 25 ± 2°C.

Instrumentation

A VITSIL-VBSD/VBDD water purification chamber was used to obtain distilled water. A CHI-6038E (CH Instruments, USA) was used to examine IC in an electrochemical chamber, having three electrodes, such as working sensors [P(GA)LMWCNTPE and MWCNTPE], a platinum electrode (counter electrode), and a saturated calomel electrode (SCE) (reference electrode). An EQ-610 digital pH instrument was used to obtain different pH values of the phosphate-buffered saline (PBS). A spectrochemical analyser (Ocean Insight, USA) was used to obtain the UV–visible spectra of IC. Field emission scanning electron microscopy (FE-SEM) (operating in keV) was used for the surface analysis of the electrode, and data were

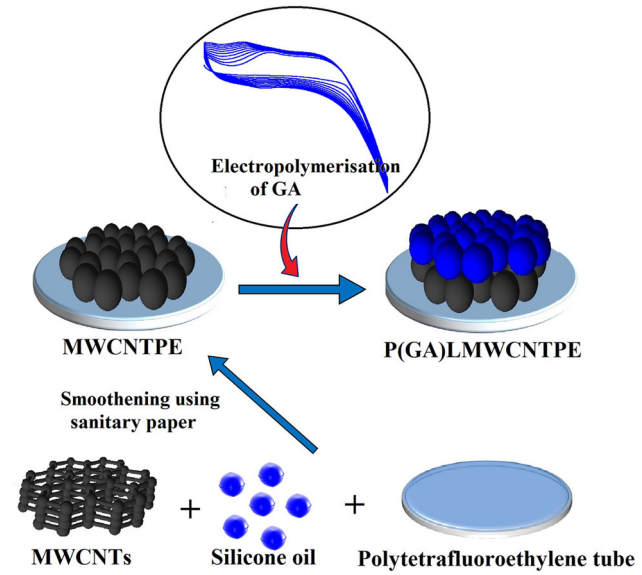

Scheme 1. Graphic representation of the preparation of electrodes.

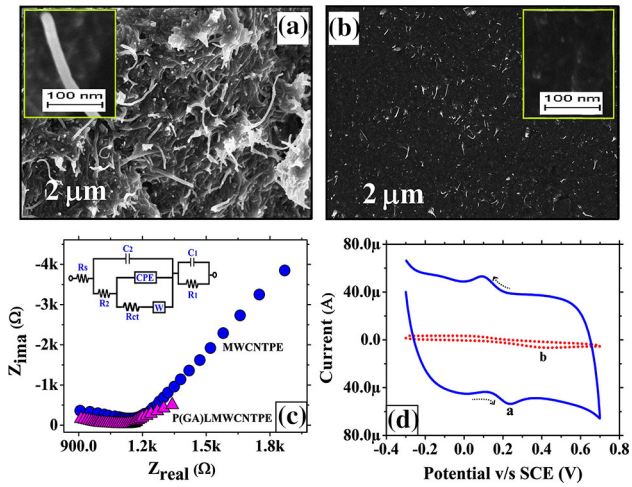

Fig. 1. FE-SEM images of the (a) MWCNTPE and (b) P(GA)LMWCNTPE. (c) EIS for 1.0 mM $K_4[Fe(CN)_6]\cdot 3H_2O$ in 0.1 M KCl at the surface of the MWCNTPE and P(GA)LMWCNTPE. (d) CV for 0.1 mM $K_4[Fe(CN)_6]\cdot 3H_2O$ in 0.1 M KCl of the P(GA)LMWCNTPE (cycle a) and MWCNTPE (cycle b) having a potential gap of −0.3 to 0.7 at a scan rate of 0.1 V/s.

obtained from the DST-PURSE Laboratory, Mangalore University, India.

Analytical Sample Preparation

The testing sample was prepared by gathering the outer shells of the Gems chocolates and then dissolved in distilled water with constant stirring to get a pure homogeneous solution. Then, the achieved solution was filtered using Whatman filter paper, and the filtrate was centrifuged. The obtained supernatant solution was collected and analysed.

Preparation of MWCNTPE and P(GA)LMWCNTPE

MWCNT powder and silicone oil were blended well in a percentage ratio of 60:40 for 15 min to attain a fine homogeneous paste. A portion of the ensuing paste was crammed into the 3-mm-diameter cavity of the polytetrafluoroethylene tube with copper wire to afford the electrical connection. The exterior of the electrode was smoothed vigilantly using a soft sanitary paper to obtain an unmodified MWCNTPE.

The freshly prepared MWCNTPE was chemically modified by the electrochemical polymerization process using 1.0 mM GA in 0.1 M PBS of 7.0 pH through the CV (10 cycles) approach by maintaining the potential gap of −0.5 V to 1.8 V at a scan rate of 0.1 V/s. After the complete electrochemical polymerization of GA on the MWCNTPE surface, we obtained the chemically modified P(GA)LMWCNTPE. Afterward, the surface of the equipped electrode was just rinsed with distilled water (to remove contamination) to get a fresh electrode surface. The graphical representation of the preparation of electrodes is shown in Scheme 1.

Table I. EIS outcomes of the MWCNTPE and P(GA)LMWCNTPE

	Working electrode	
Physical term	**MWCNTPE**	**P(GA)LMWCNTPE**
C_2 (F)	8.783×10^{-8}	9.311×10^{-7}
R_{ct} (Ω)	1.765×10^{5}	2.030×10^{-2}

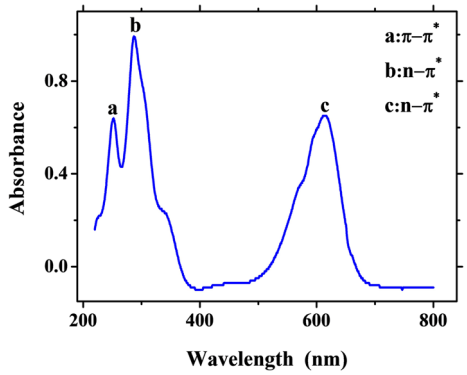

Fig. 2. UV–visible absorbance spectra for 10 µM IC in 0.1 M PBS.

RESULTS AND DISCUSSION

Surface Morphology, Conductivity, and Active Surface Area of the MWCNTPE and P(GA)LMWCNTPE

The surface morphology, conductivity, and surface area of the modified and unmodified electrodes were investigated through FE-SEM, electrochemical impedance spectroscopy (EIS), and CV performance.

The FE-SEM approach was functionalised for surface morphological study of the MWCNTPE and P(GA)LMWCNTPE. The obtained FE-SEM images are shown in Fig. 1a and b, respectively. Figure 1a presents two images with size of 2 µm and 100 nm; the 2 µm picture shows a randomly scattered bulky root-like arrangement, and the 100 nm image shows exactly a tube shape, confirming that the electrode surface comprised only MWCNTP material. Inversely, Fig. 1b displays the morphology of the P(GA)LMWCNTPE, where the surface is almost enclosed by poly(GA) films on the surface of MWCNTs (100 nm image). Hence, the modification effect increases the additional surface area for the detection of IC.

EIS is a simple methodology for the investigation of conductivity and electrocatalytic nature of the MWCNTPE and P(GA)LMWCNTPE. This study was done using 1.0 mM $K_4[Fe(CN)_6]\cdot 3H_2O$ as a testing sample in 0.1 M KCl (supporting electrolyte) in optimum conditions. According to the equivalent circuit model, the Nyquist plots display the fitting of obtained experimental EIS results for the

MWCNTPE and P(GA)LMWCNTPE (inset Fig. 1c). Here, the equivalent circuit model encloses different parameters including W (Warburg impedance) related to the diffusion-kinetic step; R_s corresponds to the electrolyte solution resistance, R_{ct} is associated with the electrode charge transfer resistance, CPE relates to the constant phase element of conductance, C_1 and C_2 correspond to the outer and inner capacitances, and R_1 and R_2 correspond to the outer and inner resistance, respectively. Nyquist plots of the MWCNTPE and P(GA)LMWCNTPE show dual-frequency sections. The initial frequency region of the MWCNTPE results the capacitance (straight line), and the higher-frequency region of the MWCNTPE results the value of R_{ct}, whereas the P(GA)LMWCNTPE displays a straight line with a small curve that symbolises the high capacitance and lower R_{ct}. The obtained R_{ct} and capacitance values are tabulated in Table I, indicating that surface activation of the MWCNTPE through electropolymerization of GA was done effectively with an efficient elevation of electrocatalytic and conductive behaviours.

The active surface area of the P(GA)LMWCNTPE and MWCNTPE is helpful for explaining the conductivity of the electrodes, and the values were estimated using the Randles–Sevcik equation.[32] Figure 1d shows the cyclic voltammograms for 0.1 mM $K_4[Fe(CN)_6]\cdot 3H_2O$ in 0.1 M KCl at both the P(GA)LMWCNTPE (cycle a) and the MWCNTPE (cycle b) with the potential window of −0.3 V to 0.7 V at a scan rate of 0.1 V/s. On the surface of the P(GA)LMWCNTPE, $K_4[Fe(CN)_6]\cdot 3H_2O$ shows faster redox action with an improved peak current with more active spots as compared to the MWCNTPE, which depends on the active surface area of the sensors.

$$I_p = 2.69 \times 10^5 n^{3/2} A D^{1/2} C \upsilon^{1/2} \quad (1)$$

where I_p represents the peak current (μA), A signifies the active surface area of the sensor (cm^2), n indicates the number of electrons, D represents the diffusion coefficient (cm^2/s), υ specifies the scan rate (mV/s), and C designates the analyte concentration (mM). The active surface area of the P(GA)LMWCNTPE and MWCNTPE was calculated using Eq. 1, and the deliberated values are 0.074 cm^2 and 0.021 cm^2, respectively. This data portrays that the formation of GA polymer films on the MWCNTPE surface increases its sensing capacity with high catalytic activity.

UV–Visible Spectra for IC

UV–visible spectrum study is a broadly used approach for the confirmation of dye light absorption behaviours. Figure 2 displays the UV–visible spectrum for 10 μM IC (in 0.1 M PBS) recorded in the spectral wavelength range of 220 nm to 800 nm. Here, IC displays three absorption peaks, two peaks in the UV region ('*a*' and '*b*') and one peak in the visible region ('*c*'), corresponding to different wavelengths 252 nm, 290 nm, and 616 nm, respectively. Additionally, these absorption peaks are due to the presence of chromophore centres followed by π–π^*, n–π^*, and n–π^* transitions, respectively. The UV region provides the maximum absorption at 290 nm, which is due to the presence of an indigoid functional group.

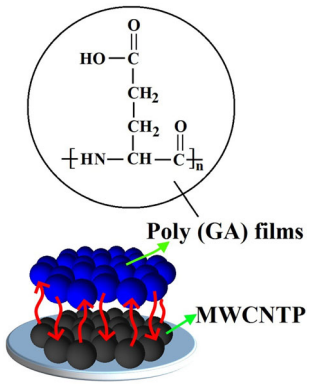

Scheme 2. The probable electrochemical polymerization reaction of GA at the surface of the MWCNTPE.

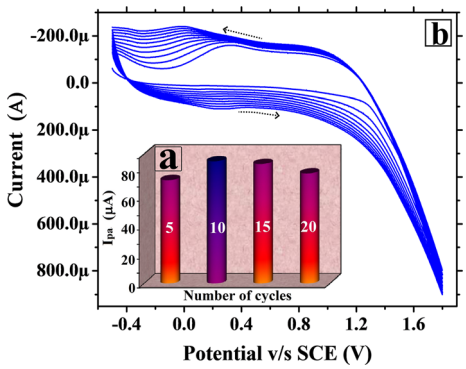

Fig. 3. (a) CVs for the electrochemical polymerization of 1.0 mM GA in 0.1 M PBS (pH 7.0) at the MWCNTPE having the potential window of −0.5 V to 1.8 V at a scan rate of 0.1 V/s. (b) Graph of a number of CV cycles against I_{pa}.

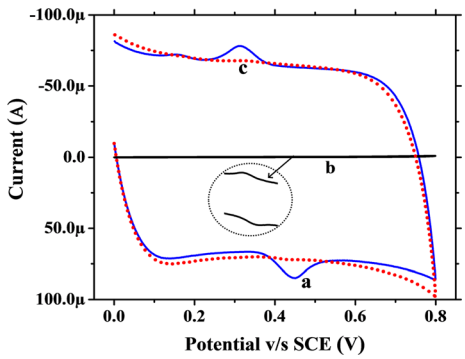

Fig. 4. CVs for the absence (cycle c) and presence of 0.1 mM IC in 0.1 M PBS (pH 7.0) at a scan rate of 0.1 V/s at the P(GA)LMWCNTPE (cycle a) and MWCNTPE (cycle b).

Electrochemical Polymerization of GA on MWCNTPE

To achieve the electropolymerization of GA on the less electroactive surface of the MWCNTPE, initially, we fixed the optimum number of CV cycles for the polymerization of GA. Figure 3a corresponds to the plot of CV cycles (5 to 20 cycles) on the MWCNTPE against the peak current of IC in 0.1 M PBS. Here, ten CV cycles provide the finest peak current response with high sensitivity for the redox action of IC as compared to 5, 15, and 20 cycles, which is possibly because of the complete coverage of poly(GA) films at the vacant surface area of the MWCNTPE. Thus ten cycles were chosen as the optimum for the polymerization of GA on the MWCNTPE. Figure 3b represents the ten CV cycles scanned with the potential gap of −0.5 V to 1.8 V at a scan rate of 0.1 V/s for the electrochemical polymerization of 1.0 mM GA in 0.1 M PBS of 7.0 pH on the MWCNTPE. The CV plot (Fig. 3b) indicates that the peak current was decreased with the increase of each CV cycle, indicating the conversion of a monomer film of GA into a polymer film of GA on the surface of the MWCNTPE. The probable reaction mechanism of poly(GA) on the MWCNTPE is shown in Scheme 2.

Electrocatalytic Behaviour of the Sensors Towards IC

The electrocatalytic activities of the MWCNTPE and P(GA)LMWCNTPE towards the electrochemical redox action of IC in PBS were analysed by CV. CVs were recorded for P(GA)LMWCNTPE and MWCNTPE in the presence and absence of IC in 0.1 M PBS of 7.0 pH at a scan rate of 0.1 V/s (Fig. 6). As evident from Fig. 4, the P(GA)LMWCNTPE (cycle a) affords a more elevated redox peak current than the MWCNTPE (cycle b) for IC with the change in potential (ΔE_p), and the anodic and cathodic peak current ratios (I_{pa}/I_{pc}) were 0.1308 V and 1.08, respectively, which defines a quasi-reversible nature. But in the case of only PBS on the surface of the P(GA)LMWCNTPE (cycle c), it does not reveal any electrochemical behaviour. As per the achieved data, the superior electrochemical redox character of IC with faster electron transfer at the surface of the P(GA)LMWCNTPE is due to the elevated active surface area, conductivity, and electrochemical modification.

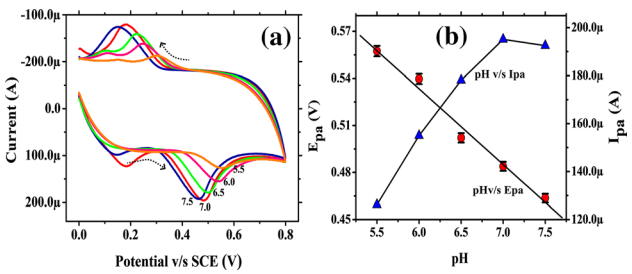

Fig. 5. (a) CVs for 0.1 mM IC at the P(GA)LMWCNTPE in 0.1 M PBS of different solution pH in the range of 5.5 to 7.5 at a scan rate of 0.1 V/s. (b) Graph of E_{pa} versus pH and I_{pa} versus pH.

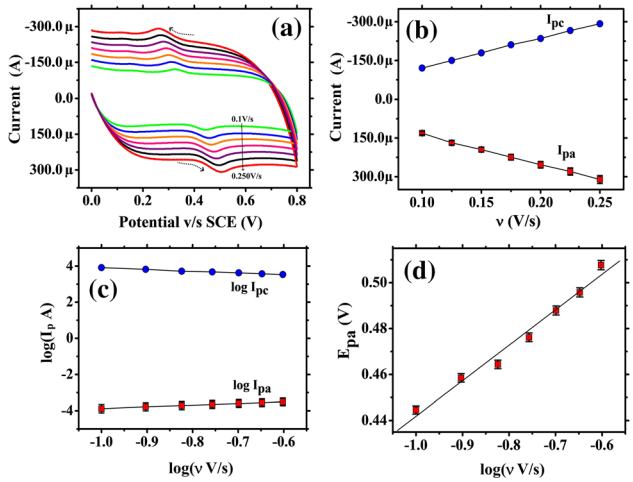

Fig. 6. (a) CVs for 0.1 mM IC in 0.1 M PBS (7.0 pH) on the P(GA)LMWCNTPE at different scan rates in the range of 0.10 V/s to 0.250 V/s. (b) Plot of peak current versus v. (c) Plot of log I_p versus log v. (d) Plot of E_{pa} versus log v.

Impact of Electrolyte pH

The impact of the functioning parameter, electrolyte pH, on the redox activity of 0.1 mM IC on the surface of the P(GA)LMWCNTPE was analysed using the CV method. The CVs were obtained for IC in altered pH of PBS in the range of 5.5 to 7.5 at the P(GA)LMWCNTPE (Fig. 5a), where we observed higher and lower percentages of proton concentration degrade the redox peak current of IC. Also, a neutral pH of 7.0 provides easy adsorption, oxidation, and reduction of IC with a high peak current on the surface of the P(GA)LMWCNTPE with a high rate of catalytic activity, as compared to other pH values (plot of pH versus I_p in Fig. 5b). Hence, pH 7.0 was selected as the optimum for the entire experiment. From the plot of pH versus E_p (Fig. 5b), a negative linear shift was observed in the oxidation peak potential of IC during the escalation of solution pH. This was demonstrated by the linear regression equation (LRE) of E_p (V) = 0.825 − (0.050) pH (V/pH) (R^2 = 0.991), with a fine linear regression coefficient (R^2), representing that the electron transfer during the oxidation and reduction of IC most probably depends on protonation. The involved protons (m) in the IC redox reaction were calculated based on pH versus E_p through $\Delta E_p/\Delta pH = 0.059\ m/\alpha n$ relation. The value of m is found to be 1.723 (nearly equal to 2), signifying that the IC redox nature is most possibly happening through the transfer of two protons and two electrons.

Scan Rate Impact on Peak Current and Potential

The inset of Fig. 6 represents the scan rate impact for 0.1 mM IC in 0.1 M PBS of 7.0 pH on the

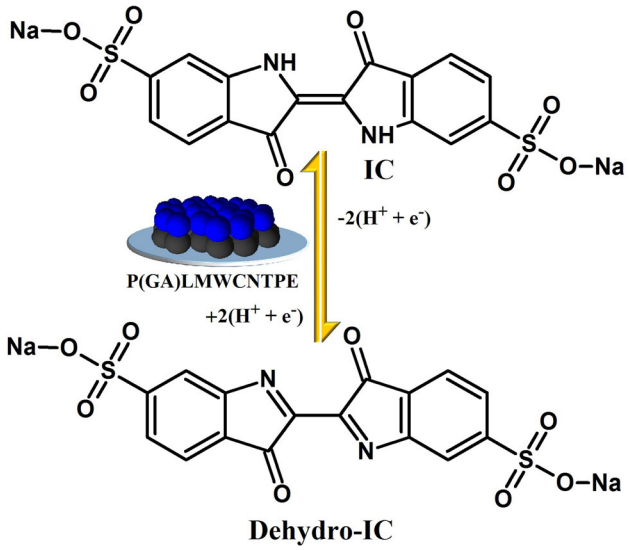

Scheme 3. The probable redox reaction mechanism of IC on the P(GA)LMWCNTPE.

P(GA)LMWCNTPE to realize the dependability of the redox nature of current and potentials on the variable scan rate. CVs obtained for IC at the altered scan rate (in the range from 0.1 to 0.25 V/s) in PBS on the active surface of the P(GA)LMWCNTPE are shown in Fig. 6a. The obtained IC oxidation peak currents and increased scan rates were proportional to one another with a fine linearity (Fig. 6b), and the slope (1.28) of log v versus log I_{pa} plot (Fig. 6c) was nearly equal to the theoretical value. This suggests that the electrode catalytic activity towards IC was predominant through adsorption-controlled kinetics, and the achieved LREs were fitted to be I_{pa} (A) = $-26.09 \times 10^{-6} + 1.24 \times 10^{-3}$ υ (V/s) (R^2 = 0.996) and log(I_{pa}, A) = $-2.81 + 1.28$ log(υ, V/s) (R^2 = 0.991). As from Fig. 6d, log υ and E_{pa} are proportional to each other with a fine linear relationship, and the achieved LRE is E_p (V) = 0.58 + 0.15 log(υ, V/s) (R^2 = 0.986). The obtained plot of E_p versus log υ was significantly used for the inspection of the number of electrons that participated in the IC redox reaction through Laviron's relationship shown as follows:[33]

$$E_p = E^0 + \left[\frac{2.303RT}{\alpha nF}\right] \log\left[\frac{RTk^0}{\alpha nF}\right] + \left[\frac{2.303RT}{\alpha nF}\right] \log \upsilon \quad (2)$$

where n is the number of electrons involved in the redox reaction of IC, E^0 is the standard redox potential (V), α is the charge transfer coefficient, E_p is the peak potential (V), k^0 is the heterogeneous rate constant (/s), T is the absolute temperature (298 K), F is the Faraday constant (96,485 C/mol), R is the universal gas constant (8.314 J/mol/K), and v is the scan rate (V/s). The calculated value of transferred electrons in the IC redox reaction was 2.26 (nearly equal to 2). The probable redox reaction

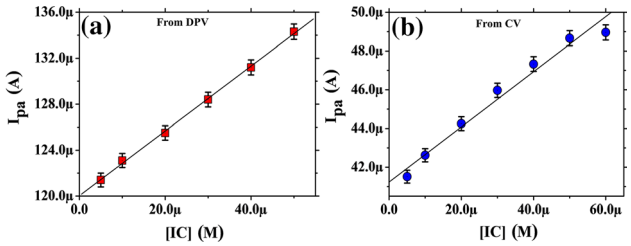

Fig. 7. (a) Graph of concentration of IC versus DPV current (I_{pa}). (b) Graph of concentration of IC versus CV current (I_{pa}).

mechanism of IC on the P(GA)LMWCNTPE is shown in Scheme 3.

The surface concentration of IC at the MWCNTPE and P(GA)LMWCNTPE was determined by the following equation:

$$\Gamma = Q/nFA \quad (3)$$

where Γ is the surface concentration of IC (M/cm^2), A is the active surface area of the MWCNTPE and P(GA)LMWCNTPE (cm^2), and Q is the charge at the anodic peak (C). The projected values of the surface concentration of the IC on the surface of the MWCNTPE and P(GA)LMWCNTPE are 0.83 Å M/cm^2 and 2.19 Å M/cm^2, respectively. Hence, the modified P(GA)LMWCNTPE shows a higher current sensitivity and faster rate of electron movement in the redox action of IC than the unmodified MWCNTPE.

Limit of Detection, Quantification, and Sensitivity

In the optimal circumstances, the limit of detection (LOD) and the limit of quantitation (LOQ) of IC at the proposed sensor were determined through DPV and CV methods by construction of a calibration curve. Differential pulse voltammograms (DPVs) were documented during the increased IC concentration in 0.1 M PBS (pH 7.0). The linear relation between the concentration and peak current of IC were achieved with acceptable linearity, and the LRE is I_{pa} (A) = $1.200 \times 10^{-4} + 0.282$ [IC] (M) (R^2 = 0.999) (Fig. 7a). Also, the same experimentation was done through the CV method for the concentration variation of IC, which provides a good linear relation with the peak current, and the corresponding LRE is I_{pa} (A) = $4.129 \times 10^{-5} + 0.1406$ [IC] (M) (R^2 = 0.989) (Fig. 7b). The LOD and LOQ values were calculated by the relations LOD = 3 SD/M and LOQ = 10 SD/M, where SD represents the standard deviation of the blank, and M signifies the slope of I_{pa} versus [IC]. From the DPV method, calculated values of LOD and LOQ were found to be 0.36 μM and 1.20 μM, and from the CV method, deliberated LOD and LOQ values were found to be 4.2 μM and 14.22 μM, correspondingly. A comparison of the currently equipped sensor with previously reported sensors for the analysis of IC is tabulated in Table II[34,35] It was concluded that the

Table II. Comparison of reported LODs, techniques, and sensors with present work

Technique	Sensor	Linear range (μM)	LOD (μM)	Reference
SERRS[1]	Silver colloids	1.0–0.1 (632.8)	36.50	34
		10.0–0.1 (514.5)	23.60	
		1.0–0.1 (514.5[c])	32.25	
		10.0–0.1 (632.8)	28.00	
		10.0–0.1 (632.8[c])	19.50	
LC-APCI-MS[2]	–	10–100	29.00	35
DPV	P(GA)LMWCNTPE	5.0–50.0	0.36	Present study
CV		5.0–60.0	4.20	

[1] Surface-enhanced resonance Raman spectroscopy.
[2] Liquid chromatography-atmospheric pressure chemical ionization-mass spectroscopy.

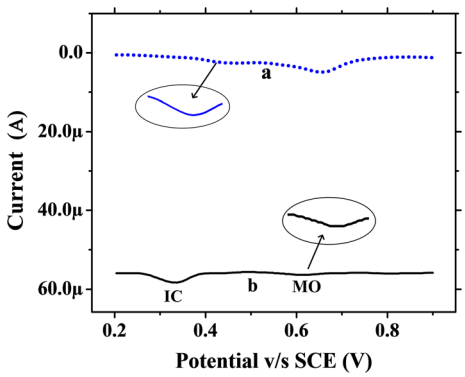

Fig. 8. DPVs for 0.05 mM IC in the presence of 0.05 mM MO in 0.1 M PBS (7.0 pH) on the surface of the MWCNTPE (cycle a) and P(GA)LMWCNTPE (cycle b) at an amplitude of 0.05 V and pulse period of 0.5 s.

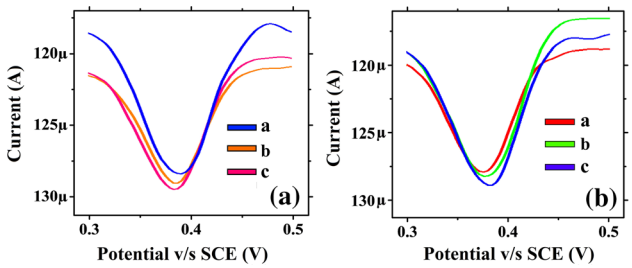

Fig. 9. DPVs for the analysis of IC in (a) food sample and (b) water sample at different concentrations in 0.1 PBS of 7.0 pH.

projected sensor affords a better electrocatalytic response for IC detection by DPV method with a lower LOD. The sensitivity of the P(GA)LMWCNTPE was calculated by the use of the active surface area of the sensor and the slope of the calibration plot (from DPV), and the calculated value is 3.81 A/M/cm^2.

Simultaneous Analysis

DPV was utilised for the examination of selectivity of the MWCNTPE and P(GA)LMWCNTPE towards 0.05 mM IC in the presence of 0.05 mM MO. As evident from Fig. 8, the MWCNTPE discloses less sensible anodic peaks for IC and MO, but the P(GA)LMWCNTPE shows fine distinct anodic peaks with high current for IC and MO, respectively. The obtained data elucidates that the high electrocatalytic action of the P(GA)LMWCNTPE for IC in the presence and absence of MO is almost alike, thus the redox behaviour of IC and oxidative nature of MO on the surface of P(GA)LMWCNTPE are dissimilar and subsequently simultaneous. Therefore, the projected P(GA)LMWCNTPE is completely free from the interfering molecules.

Storage Stability and Reproducibility

The storage stability of the P(GA)LMWCNTPE for the analysis of IC in PBS was inspected through CV method by preserving the sensor for 6 days in a sealed container. The deliberated value of percentage degradation demonstrates 88.88% of the initial peak current even after 6 days, which affords acceptable storage stability of the sensor. The reproducibility of the sensor was estimated by cycling CV on constant IC in PBS at ten separately modified sensors. Here, the equipped sensor provides the relative standard deviation (RSD) of 3.83%, demonstrating fine reproducibility.

Analysis of Food and Water Samples

To validate the proposed P(GA)LMWCNTPE for the testing of real samples, the implemented sensor and DPV technique were applied for the examination of IC in food and water samples. The analysis of IC was done by the standard spike recovery approach for both food and water samples, individually. The obtained DPVs for both food (a = 0.1 mM, b = 0.15 mM, and c = 0.2 mM) and water (a = 0.1 mM, b = 0.15 mM, and c = 0.2 mM) samples are displayed in Fig. 9a and b, respectively. The P(GA)LMWCNTPE provides recoveries of 99.06 to 99.76% (in food samples) and 98.91% to 99.61% (in water samples) with fine RSDs. The found results are tabulated in Table III. The obtained data reveal that the proposed sensor is the correct choice for IC analysis in both food and water samples with fine recovery and an acceptable RSD.

Table III. Recovery data of IC in food and water samples

Analytical sample	Spiked concentration (μM)	Found concentration (μM)	Recovery (%)	RSD (%)
Food sample (Gems chocolate)	2.140	2.120	99.06	3.16
(n = 3)	3.210	3.200	99.68	
	4.280	4.270	99.76	
Water sample (n = 3)	10.000	9.891	98.91	3.26
	15.000	14.872	99.14	
	20.000	19.922	99.61	

CONCLUSIONS

In this work, a fine sensitive and selective electrochemically polymerised GA film-based carbon nanotube sensor was fabricated efficaciously for the analysis of IC redox behaviours with MO. The projected P(GA)LMWCNTPE portrays a very good electrocatalytic nature as compared to the unmodified electrode for the redox reaction of IC trough CV and DPV methods. The surface area calculation and EIS show that the P(GA)LMWCNTPE has more surface sites with high conductive strength. The solution pH and scan rate parameters reveal that the developed electrode shows adsorption-controlled kinetics with the transfer of two electrons and two protons during the reduction of IC in PBS. Moreover, the P(GA)LMWCNTPE affords considerable linear relations in both CV and DPV methods with lower LODs. Based on these data, the P(GA)LMWCNTPE is an advantageous tool for the investigation of IC in food and water samples with good recovery.

ACKNOWLEDGMENTS

We thankfully acknowledge the financial support from VGST, Bangalore under the Research Project No. KSTePS/VGST-KFIST(L1)2016-2017/GRD-559/2017-18/126/333, 21/11/2017, and the Department of Science and Technology (DST) for the INSPIRE Fellowship (Registration Number: IF180479).

CONFLICT OF INTEREST

This work has no conflict of interest.

REFERENCES

1. J.G. Manjunatha, *J. Food Drug Anal.* 26, 292 (2018).
2. K. Hunger, *Industrial Dyes: Chemistry, Properties, Applications*, 1st ed. (New York: Wiley, 2007), pp. 1–10.
3. E. Gurr, *Synthetic Dyes in Biology, Medicine and Chemistry*, 1st ed. (Amsterdam: Elsevier, 2012), pp. 1–11.
4. G. McMullan, C. Meehan, A. Conneely, N. Kirby, T. Robinson, P. Nigam, I. Banat, R. Marchant, and W. Smyth, *Appl. Microbiol. Biotechnol.* 56, 81 (2001).
5. F.M.D. Chequer, G.A. Rodrigues de Oliveira, E.R.A. Ferraz, J.C. Cardoso, M.V.B. Zanoni, and D. Palma de Oliveira, *IntechOpen.* (2013). https://doi.org/10.5772/53659.
6. S. Ammar, R. Abdelhedi, C. Flox, C. Arias, and E. Brillas, *Environ. Chem. Lett.* 4, 229 (2006).
7. K. Ikeda, Y. Sannohe, S. Araki, and S. Inutsuka, *Gastrointest. Endosc.* 26, 19801 (1980).
8. J.E. Song and S.K. Kim, *J. Urol.* 98, 669 (1967).
9. M. Altok, A.F. Sahin, M.I. Gokce, G.R. Ekin, and R.T. Divrik, *Int. Braz. J. Urol.* 43, 1052 (2017).
10. M. Fujita, C. Kuroda, N. Hosomi, E. Inoue, K. Kuriyama, H. Ohhigashi, S. Kishimoto, O. Ishikawa, and A. Nakaizumi, *J. Vasc. Interv. Radiol.* 6, 119 (1995).
11. W. Fao, Codex Alimentarius Commission, Safety of Colors, GSFA MPLs of Indigo Carmine (2015), p. 132.
12. J. Naitoh and B.M. Fox, *Urology.* 44, 271 (1994).
13. T.Y. Ng, T.D. Datta, and B.I. Kirimli, *J. Urol.* 116, 132 (1976).
14. U.R. Lakshmi, V.C. Srivastava, I.D. Mall, and D.H. Lataye, *J. Environ. Manag.* 90, 710 (2009).
15. W.K. Kennedy, K. Wirjoatmadja, T.J. Akamatsu, and J.J. Bonica, *J. Urol.* 100, 775 (1968).
16. M.S. Secula, I. Cretescu, and S. Petrescu, *Desalination* 277, 227 (2011).
17. P.A. Pushpanjali, J.G. Manjunatha, C. Raril, and D.K. Ravishankar, *RJLBPCS.* 5, 820 (2019).
18. A. Mittal, J. Mittal, and L. Kurup, *J. Hazard. Mater.* 137, 591 (2006).
19. T.H. Fereja, S.A. Kitte, M.N. Zafar, M.I. Halawa, S. Han, W. Zhang, and G. Xu, *Analyst.* 145, 1041 (2020).
20. H. Oka, Y. Ikai, K. Kawamura, M. Yamada, and H. Inoue, *J. Chromatogr. A* 411, 437 (1987).
21. K.S. Minioti, C.F. Sakellariou, and N.S. Thomaidis, *Anal. Chim. Acta* 583, 103 (2007).
22. J.J. Berzas, J.R. Flores, M.J.V. Llerena, and N.R. Farinas, *Anal. Chim. Acta* 391, 353 (1999).
23. C.F. Tsai, C.H. Kuo, and D.Y.C. Shih, *J. Food Drug Anal.* 23, 453 (2015).
24. M.J.B. Alvarez, M.T.F. Abedul, and A.C. Garcia, *Anal. Chim. Acta* 462, 31 (2002).
25. G.K. Jayaprakash, B.E. Kumara Swamy, J.P. Mojica Sanchez, X. Li, S.C. Sharma, and S.L. Lee, *J. Mol. Liq.* 315, 113719 (2020).
26. J.G. Manjunatha, *Sens. Biosens. Res.* 16, 79 (2017).
27. G.K. Jayaprakash, B.E. Kumara Swamy, S.C. Sharma, and J.J. Santoyo-Flores, *Microchem. J.* 158, 105116 (2020).
28. N. Hareesha and J.G. Manjunatha, *Mater. Res. Innov.* 24, 349 (2019). https://doi.org/10.1080/14328917.2019.1684657.
29. G.K. Jayaprakash, B.E.K. Swamy, N. Casillas, and R. Flores-Moreno, *Electrochim. Acta* 248, 225 (2017).
30. B.M. Amrutha, J.G. Manjunatha, S. Aarti Bhatt, and N. Hareesha, *J. Mater. Environ. Sci.* 10, 668 (2019).
31. Z. Fan, P. Cheng, M. Liu, D. Li, G. Liu, Y. Zhao, Z. Ding, F. Chen, B. Wang, X. Tan, Z. Wang, and J. Han, *New J. Chem.* 41, 8656 (2017).
32. N. Hareesha and J.G. Manjunatha, *J. Iran. Chem. Soc.* 17, 1507 (2020).
33. E. Lavirons, *J. Electroanal. Chem.* 52, 355 (1974).
34. I.T. Shadi, B.Z. Chowdhry, M.J. Snowden, and R. Withnall, *Spectrochim. Acta A* 59, 2213e20 (2003).
35. B.C. Liau, T.T. Jong, and S.S. Chen, *J. Pharm. Biomed.* 43, 346 (2007).